Available online at www.sciencedirect.com

SciVerse ScienceDirect

www.elsevier.com/locate/matchar

Microstructural evolution of fusion zone in laser beam welds of pure titanium

H. Liu[a,b,*], K. Nakata[b], J.X. Zhang[a], N. Yamamoto[c], J. Liao[c]

[a]State Key Laboratory for Mechanical Behavior of Materials, Xi'an Jiaotong University, Xi'an 710049, China
[b]Joining and Welding Research Institute, Osaka University, Ibaraki 567-0047, Japan
[c]Technology Development Headquarters, Kurimoto Ltd., Osaka 559-0021, Japan

ARTICLE DATA

Article history:
Received 29 July 2011
Received in revised form
21 December 2011
Accepted 22 December 2011

Keywords:
Phase transformation
Microstructural evolution
Laser beam weld
Pure titanium

ABSTRACT

Microstructural evolution of fusion zone in laser beam welds of pure titanium was studied by means of electron backscattering diffraction. The microstructural evolution is strongly affected by the $\beta \rightarrow \alpha$ transformation mechanism dependent on the cooling rate during phase transformation. The long-range diffusional transformation mainly occurs in the fusion zone at the low cooling rate, and the massive transformation dominantly takes place at the high cooling rate. For this reason, the grain morphologies probably change from the granular-like to columnar-like grains with the cooling rate increasing.

1. Introduction

The welding and joining of titanium and its alloys have gained considerable interests in order to apply these materials to various products. A great number of researches have been conducted to the fusion welding techniques recently [1–7], especially to the laser beam welding (LBW) [4,7–12]. The columnar and equiaxed grains are often the microstructural constituents in the fusion zone (FZ) of alloys [13,14]. During solidification, the columnar grains are likely formed adjacently to the heat affected zone (HAZ) by the epitaxial growth, and the equiaxed grains are usually developed in the center part of FZ by the nucleation and growth. On the other hand, only columnar grains can grow epitaxially in the FZ of pure metal, because the alloying elements are so scant that the nucleation and growth of equiaxed grains are very difficult [14]. However, the microstructural evolution in the FZ of titanium and its alloys may be remarkably different due to the occurrence of $\beta \rightarrow \alpha$ phase transformation after solidification. Unfortunately, the published works have been done in order to evaluate the design optimization of the LBW technique, and little work has reported the fundamentally physical understanding of microstructural evolution in the FZ of titanium and its alloys. In the present study, the laser beam welds of pure titanium were prepared under various welding conditions, and the microstructural evolution of FZ was investigated in detail.

2. Experimental

The as-received material was a grade 2 commercially pure titanium sheet with shape dimensions of 300×100×4 mm and chemical compositions of Ti—0.004C–0.0023H–0.078O–0.006N–0.048Fe (wt.%). During welding, the workpiece was bead-on-plate welded by an IPG YLR-10000 fiber laser welding system with a beam diameter of 0.47 mm. The laser power was fixed at 10 kW and the welding speeds changed from 2 to 8 m/min. Both the top and bottom surfaces of the welds were shielded using ultra high purity argon gas (99.999%) with a

* *Corresponding author*. Tel./fax: +86 29 82668807.
E-mail address: hitliuhong@163.com (H. Liu).

1044-5803/$ – see front matter © 2011 Elsevier Inc. All rights reserved.
doi:10.1016/j.matchar.2011.12.010

flow rate of 25 L min^{-1} to minimize the surface oxidation. After welding, the laser beam welds were cross-sectioned for the metallographic analysis by a wire electrical discharge cutting machine (HSC-300; Brother Ind. Ltd). The cross-sections were mechanically polished using water abrasive papers, and then were electro-polished at room temperature for 30 s under a potential of 25 V in a solution containing perchloric acid, n-butyl alcohol and methanol at a volume ratio of 1:7:10. Finally, the polished cross-sections were etched in a solution comprising of hydrofluoric acid, nitric acid and distilled water at a volume ratio of 1:1:8. The specimens were examined by a scanning electron microscope (VE-8800; Keyence Corp.). Electron backscattering diffraction (EBSD) was realized by a scanning electron microscope (JSM-6400; JEOL Ltd.) incorporated with a TexSEM Laboratories (MSC-2200; TexSEM Laboratories Inc.). The step size of 3.0 μm was used and the average confidential index from 0.55 to 0.65 was obtained in the EBSD maps. Small grains comprising fewer pixels were removed using the grain-dilation option to ensure reliability, and the misorientation angles less than 2° were deleted to eliminate false boundaries caused by orientation noise.

3. Results and Discussion

3.1. *Microstructural Morphologies of the FZs*

Fig. 1 presents the microstructures of the vertical cross-sections in the welds of pure titanium under various welding conditions. The reference directions of the vertical cross-sections are displayed in the top right corner. The ND, TD and WD are the normal, transverse and welding directions, respectively. It can be seen that a keyhole type of penetration is detected in the welds. The fully penetrated welds with a narrow and symmetric shape are obtained in this work, which are evidently composed of the base metal (BM), the HAZ and the FZ. A clear boundary between the BM and HAZ is easily distinguished because of the microstructural difference. However, the fusion line is not accurately identified due to the similar microstructures formed in the HAZ and FZ, and thus it is approximately asserted according to the location of weld root and weld toe [3]. In order to confirm the microstructural morphologies, the microstructures of the horizontal cross-sections in the welds of pure titanium are given in Fig. 2, where the reference directions of the horizontal cross-sections are shown in the top right corner. It should be noted that the cutting positions for getting the horizontal cross-sections are described by the dotted black lines as seen in Fig. 1. As shown in Figs. 1 and 2, the microstructural morphology of the FZs obviously changes with the welding condition. The FZ dominantly consists of the granular-like grains under the welding condition of 10 kW laser power and 2 m/min welding speed, while a few columnar-like grains are also observed in the top and bottom parts of the FZ. As the welding speed is increased to be 4 m/min, many columnar-like grains appear in the top and bottom parts of the FZ, and the granular-like grains are restrictedly detected in the center part of the FZ. With the further increase of welding speed, the columnar-like grains completely dominate the microstructure of the FZ under the welding condition of 10 kW and

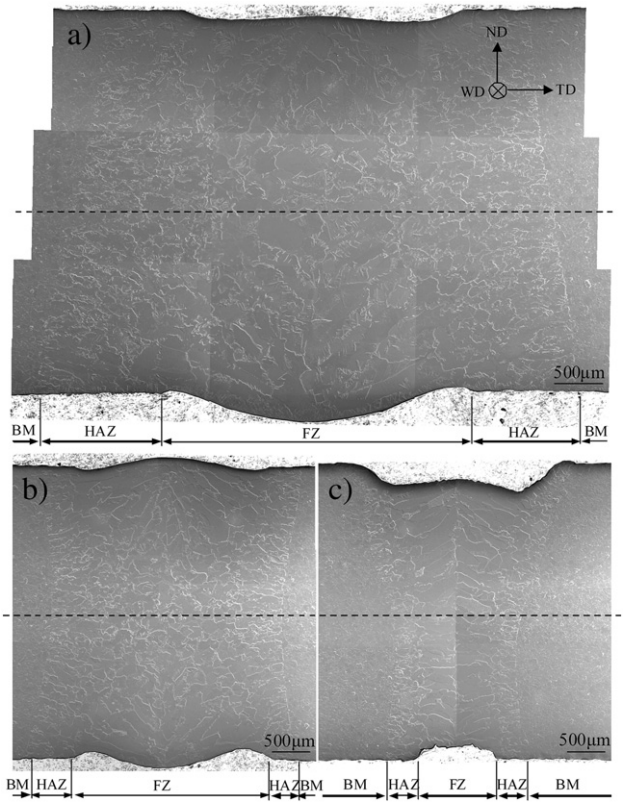

Fig. 1 – Microstructures of the vertical cross-sections in the welds under various welding conditions: (a) 10 kW–2 m/min; (b) 10 kW–4 m/min; (c) 10 kW–8 m/min.

8 m/min. It is necessary to say that the lath-like martensite is not found in the FZs. Apparently, it can be concluded that the granular-like grains are found in the FZ when the cooling rate is low and the grain morphology gradually changes from the granular-like to columnar-like one with the cooling rate increasing. This result means that the final microstructure in the FZ of laser beam welded pure titanium strongly depends on the $\beta \rightarrow \alpha$ phase transformation associated with the cooling rate, since only the columnar grains can be formed in the FZ of pure metal during solidification.

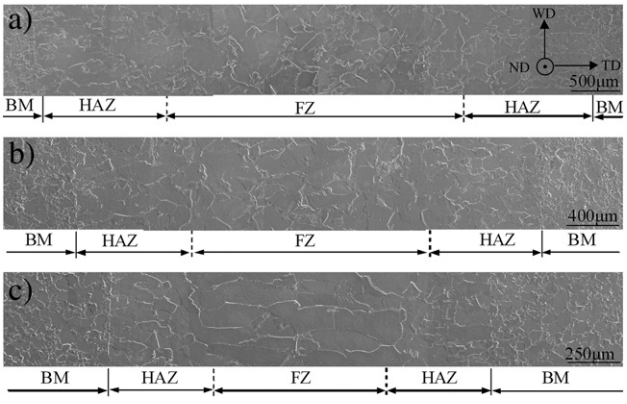

Fig. 2 – Microstructures of the horizontal cross-sections in the welds under various welding conditions: (a) 10 kW–2 m/min; (b) 10 kW–4 m/min; (c) 10 kW–8 m/min.

3.2. *Grain Orientations and Misorientation Distributions in the Welds*

The center parts of the vertical cross-sections, which exhibit the typical microstructures, are selected to investigate the microstructural evolution. The grain orientation maps under various welding conditions are given in Fig. 3, where the sample reference directions and the color code triangle are shown in the right side. The similar grain orientations are formed in the HAZ and FZ due to the occurrence of the β→α phase transformation, which are markedly different from that in the BM. Thus, a clear boundary can be found between the BM and HAZ, and the fusion line can hardly be identified between the HAZ and FZ. Moreover as seen in Fig. 3, it can be found that the granular-like grains are observed in the FZ at low cooling rate and the columnar-like grains are shown in the FZ at high cooling rate, absolutely consistent with the microstructural features shown in Figs. 1 and 2. The misorientation distributions and (0002) pole figures in the weld under the welding condition of 10 kW laser power and 4 m/min welding speed are represented in Fig. 4. A texture with a bimodal distribution of basal plane is revealed, and a lot of high-angle misorientation distributions are detected in the BM as well as the sporadic low-angle misorientation distributions. After welding, the bimodal texture completely disappears, and the special texture distributions appear in the HAZ and FZ. The results obtained by Leary et al [15] suggest that the special texture distributions in the HAZ and FZ are not extensively carried from the BM, but may still be affected by the BM. The formation mechanism of special texture distributions in the HAZ and FZ is not clear at present, and further work is required in this area. Additionally, the similarly special misorientation distributions are found in the HAZ and FZ, meaning that the complete β→α phase transformation occurs in the HAZ similar with the FZ. The misorientation distributions are characterized by a strong low-angle peak followed by three weak high-angle peaks and three wide high-angle gaps.

It is well known that the relationship between the inherited α grain and the parent β grain conforms to the Burgers relationship during β→α phase transformation [16]. Besides, the boundaries in the microstructure of pure titanium after β→α phase transformation can be divided into three kinds, which are the substructure boundaries within α grains, the α/α grain boundaries where two α grains are inherited from one parent β grain, and the α/α grain boundaries where two α grains are developed from two different β grains, respectively. Accordingly, three types of misorientation angles are described as follows based on the three different boundaries [17–20]: the misorientation angles of 2–8.029° result from the substructure boundaries within α grains (type 1); the misorientation angles around 8.029–13.029°, 57.5–65.762° and 87.5–92.5° are induced by the α/α grain boundaries where two α grains are inherited from one parent β grain in view of a tolerance of ±2.5° (type 2); the misorientation angles of 13.029–57.5°, 65.762–87.5° and 92.5–94° are caused by the α/α grain boundaries where two α grains are developed from two different β grains (type 3).

Therefore, the strong low-angle peak and three weak high-angle peaks together with three wide high-angle gaps (shown in Fig. 4b and c) are respectively accordant with the type 1, type 2 and type 3 misorientation angles mentioned above. The misorientation distributions of the FZs in the welds under various welding conditions are shown in Fig. 5, where three types of misorientation angles are displayed. The similar misorientation distributions are found in the FZs of the welds under various welding conditions. However, the fractions of type 1 and type 2 misorientation angles are visibly influenced by the cooling rate associated with the welding speed. With the welding speed increasing, the fraction of type 1 misorientation angles gradually ascends and the fraction of type 2 misorientation angles gently descends. When welded at 10 kW–8 m/min, the fraction of type 1 misorientation angles is up to 0.612 and the fraction of type 2 misorientation angles reduces to 0.217. The decreasing fraction of type 2 misorientation angles indicates that the number of α grains inherited from one parent β grain distinctly decreases with the welding speed increasing. Moreover, the type 1 misorientation angles relative to the substructure boundaries within α grains are formed due to the non-equilibrium transformation during fast cooling [18], and thus the higher fraction of type 1 misorientation angles is reasonably observed when welded at faster welding speed. It should be pointed out that

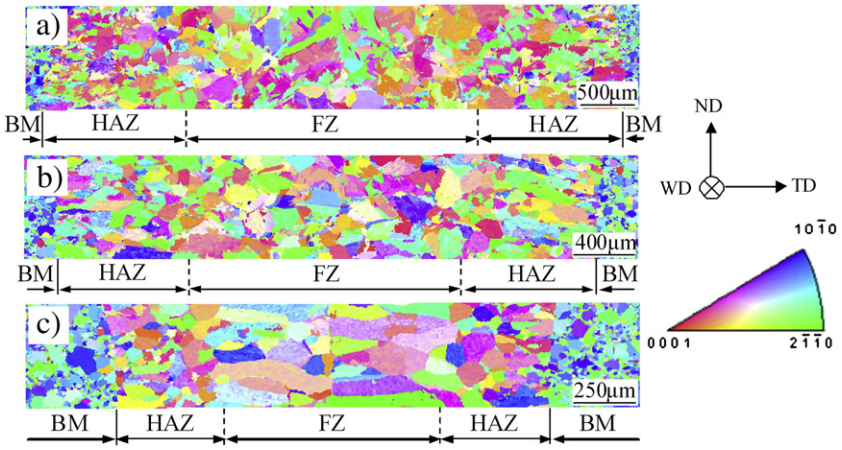

Fig. 3 – Grain orientation maps in the center parts of the vertical cross-sections under various welding conditions: (a) 10 kW–2 m/min; (b) 10 kW–4 m/min; (c) 10 kW–8 m/min.

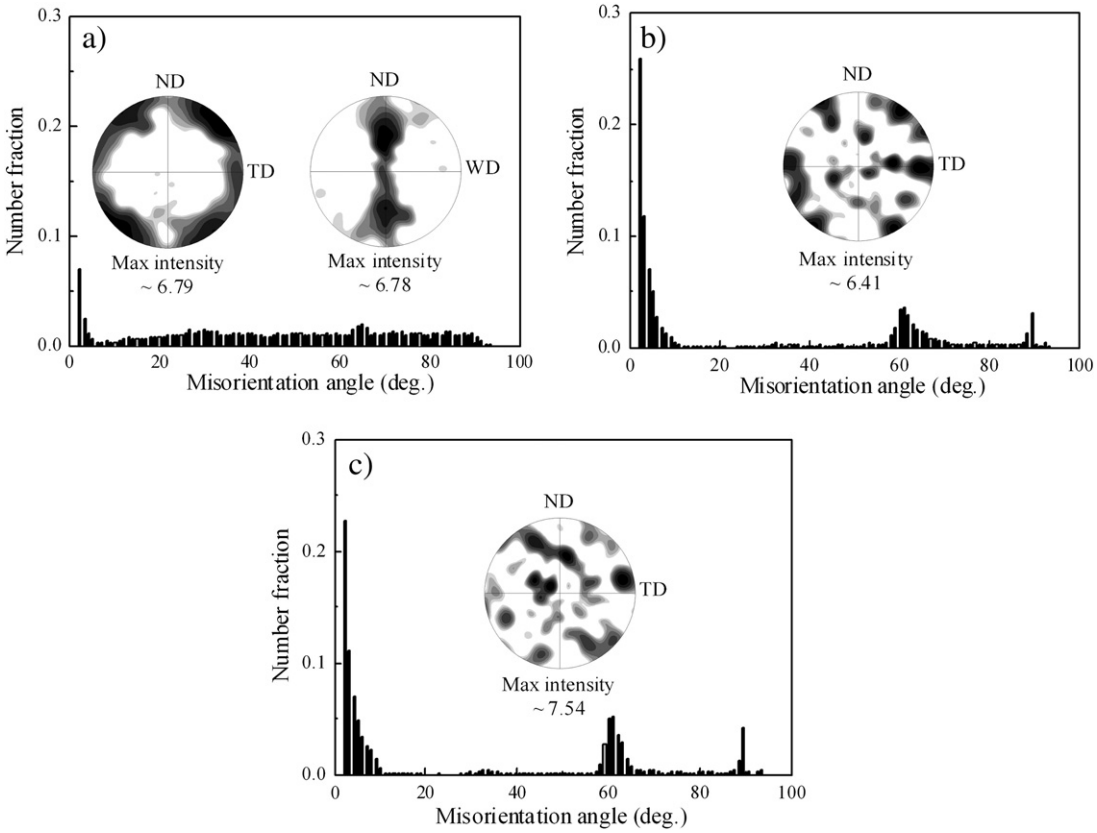

Fig. 4 – Misorientation distributions and (0002) pole figures in the weld under the welding condition of 10 kW laser power and 4 m/min welding speed: (a) BM; (b) HAZ; (c) FZ.

the α/α grain boundaries where two α grains are developed from two different β grains are considered to be the parent β grain boundaries [17]. As a result of the coarse β grains formed during welding, the low fraction of type 3 misorientation angles is found in the misorientation distributions. On the other hand, the formation of abundant substructure boundaries within α grains may also lead to the extraordinarily low fraction of type 3 misorientation angles.

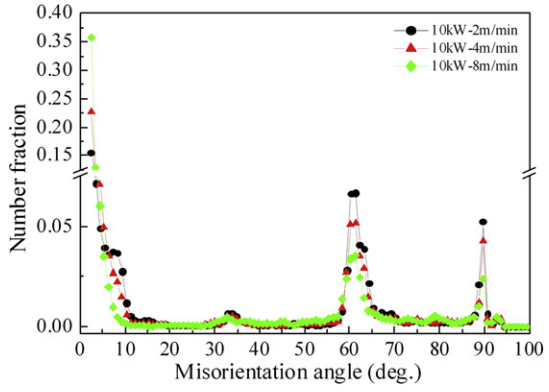

Fig. 5 – Misorientation distributions of the FZs in the welds under various welding conditions.

3.3. *Phase Transformation of the FZs*

Three kinds of β→α transformation mechanisms are observed in pure titanium, which are obviously dependent on the cooling rate during phase transformation [21,22]. They are the long-range diffusional transformation at low cooling rates, the short-range diffusional transformation (massive transformation) at medium cooling rates, and the diffusionless transformation (martensitic transformation) at high cooling rates, respectively. The critical cooling rates for these phase transformations are strongly affected by the alloying elements. The featureless patches or fine wavy acicular features are formed in the microstructure when the massive transformation occurs, completely different from the extremely fine lathlike features produced by the martensitic transformation. The grain boundary maps of the FZs under various welding conditions are given in Fig. 6. The 10° criterion is generally used to define the low-angle boundaries (LABs) with low surface energy versus the high-angle boundaries (HABs) with high surface energy. The LABs and HABs are denoted by the solid gray line and solid black line, respectively. The LABs (2–10°) are mostly composed of the boundaries (type 1, 2–8.029°), but they also contain a small quantity of the boundaries (type 2, 8.029–10°). A large number of α grains without LABs are predominately shown in the FZ under the welding condition of 10 kW laser power and 2 m/min welding speed, but a small amount of α grains with LABs is still observed in the region. With the increase of welding

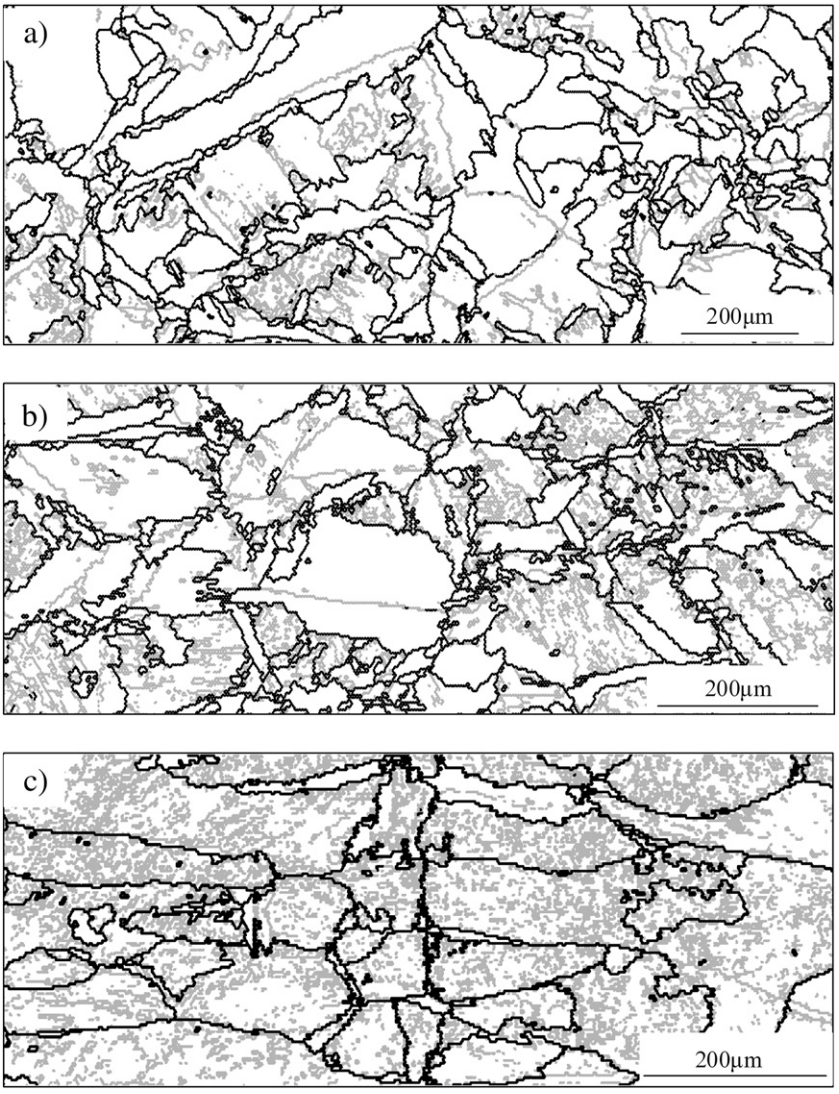

Fig. 6 – Grain boundary maps of the FZs under various welding conditions: (a) 10 kW–2 m/min; (b) 10 kW–4 m/min; (c) 10 kW–8 m/min.

speed, the number of α grains without LABs decreases and the amount of α grains with LABs sharply increases, which is consistent with the climbing trend of type 1 misorientation angles shown in Fig. 5. When the welding speed is up to 8 m/min, the α grains without LABs almost disappears, and the α grains with LABs dominate the microstructure of the FZ. As seen in Fig. 6, the fine lathlike feature is absent in the microstructures, which means that only the diffusional transformations take place in the present work. The LABs within α grains distinctly describe the featureless patches or fine wavy acicular features, highly similar with the microstructural characteristics originated from the massive transformation [21]. Besides, the LABs are commonly believed to be the relatively simple arrangements of dislocations, meaning that much more dislocations exist in the α grains with LABs compared with the α grains without LABs. In fact, a large number of dislocations have been observed in the products formed by the massive transformation [23,24].

The microstructural evolution of FZ in laser beam welds of pure titanium appears to be relative to the $\beta \rightarrow \alpha$ transformation mechanism, which is markedly dependent on the cooling rate during phase transformation. In order to confirm the transformation mechanisms, the cooling rates during phase transformation under various welding conditions are calculated by the Rosenthal's Two-Dimensional Equation [14]. Fig. 7 plots the calculated temperature profile along the centerline of the weld under the welding condition of 10 kW laser power and 2 m/min welding speed. The zone near point heat source actually accords with the position of keyhole during laser beam welding, where the temperatures reasonably exceeds the evaporation temperature of pure titanium. The cooling rate is obtained by multiplying the spatial derivative of this plot by the welding speed of the weld [25]. This calculation shows that the cooling rate during phase transformation is about 295 °C/s under the welding condition of 10 kW and 2 m/min. In the same way, the cooling rate during phase transformation arrives at 412 °C/s under the welding condition of 10 kW and 4 m/min, and it increases to 870 °C/s when the welding speed reaches 8 m/min. The range of cooling rates for massive transformation of pure titanium is significantly

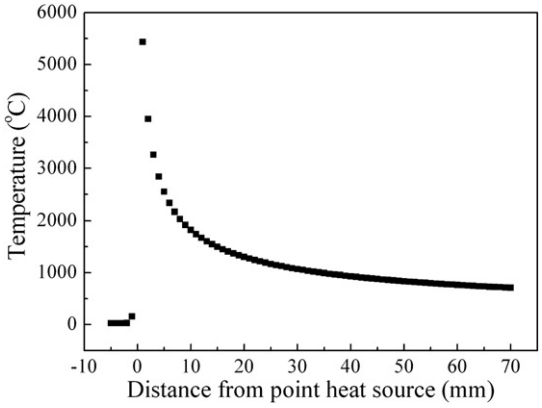

Fig. 7 – Calculated temperature profile along the centerline of the weld under the welding condition of 10 kW laser power and 2 m/min welding speed.

influenced by the iron element. The massive transformation of the extra-pure titanium (with 0.0004 wt.% Fe) occurs at the cooling rates from 350 to 1000 °C/s, the massive transformation of the grade 2 commercially pure titanium (with 0.07 wt.% Fe) appears at the cooling rates from 90 to 600 °C/s, and the massive transformation of the grade 4 commercially pure titanium (with 0.13 wt.% Fe) is strongly contracted at the cooling rates from 30 to 300 °C/s [21,22]. The massive transformation of the as-received grade 2 commercially pure titanium containing 0.048 wt.% Fe is probably expanded to the higher cooling rate (compared with the grade 2 commercially pure titanium with 0.07 wt.% Fe), and thus the calculated cooling rates in this investigation are considered to be reasonable.

Based on the discussion above, the α grains with LABs are likely ascribed to the massive transformation, whereas the α grains without LABs are probably associated with the long-range diffusional transformation. The coexistence of the α grains with LABs and the α grains without LABs is quite accordant with the fact that the massive transformation is always accompanied by the long-range diffusional transformation at low cooling rates, which has been found in the commercially pure titanium arc welds [25]. When welded at the low welding speed, the formation of plentiful α grains without LABs suggests that the phase transformation mainly occurs by the long-range diffusional mechanism due to the relatively low cooling rate. The heterogeneous nucleation of α grain firstly starts to appear in the parent β grain boundaries adjacent to the fusion line because of the special temperature distribution during welding. The nucleation phenomenon subsequently occurs in the prior β grain boundaries close to the weld center line, and the former α grains gradually grow up in the prior β grains at the same time. Therefore, many α grains are formed in the prior β grains, which change the columnar structure of the prior β grains produced during solidification. However, the α grains with LABs progressively emerge with the welding speed increasing, and they are dominantly observed in the FZ when welded at the high welding speed. It implies that the phase transformation nearly occurs by the short-range diffusional mechanism owing to the relatively high cooling rate. Similarly, the nucleation sites of this phase preferentially occur in the prior β grain boundaries near the fusion line. Dissimilarly, the massive product usually nucleates much more slowly than the precipitate product by long-range diffusion [26], and the growth rate of the massive transformation is several orders of magnitude faster than that of the long-range diffusional transformation [24,26,27]. As a result, only few α grains formed by massive transformation may rapidly occupy the prior β grains, and the columnar structure of the prior β grains is probably reserved after phase transformation. The number of the α grains formed within the prior β grains clearly decreases with the welding speed increasing, which is in good agreement with the depressed trend of type 2 misorientation angles seen in Fig. 5.

4. Conclusions

The granular-like grains are found in the FZ when the cooling rate is low, and the grain morphologies gradually change from the granular-like to columnar-like one with the cooling rate increasing. The similar grain orientations and misorientation distributions formed in the HAZ and FZ are completely different from those in the BM. According to the misorientation distributions of the FZs, the substructure boundaries within α grains gradually increase with the welding speed increasing, and the α/α grain boundaries where two α grains are inherited from one parent β grain gently decrease. The long-range diffusional transformation mainly occurs in the FZ at the low cooling rate. Many α grains are formed in the prior β grains, which changes the columnar structure of the prior β grains produced during solidification. However, the massive transformation dominantly takes place at the relatively high cooling rate. Few α grains are formed in the prior β grains, and the columnar structure of the prior β grains is reserved at room temperature.

REFERENCES

[1] Sundaresan S, Janaki Ram GD, Madhusudhan Reddy G. Microstructural refinement of weld fusion zones in α-β titanium alloys using pulsed current welding. Mater Sci Eng A 1999;262:88–100.
[2] Liu L, Du X, Zhu M, Chen G. Research on the microstructure and properties of weld repairs in TA15 titanium alloy. Mater Sci Eng A 2007;445–446:691–6.
[3] Lathabai S, Jarvis BL, Barton KJ. Comparison of keyhole and conventional gas tungsten arc welds in commercially pure titanium. Mater Sci Eng A 2001;299:81–93.
[4] Roggensack M, Walter MH, Böning KW. Studies on laser- and plasma-welded titanium. Dent Mater 1993;9:104–7.
[5] Mohandas T, Banerjee D, Mahajan YR, Kutumba Rao VV. Studies on fusion zone fracture behaviour of electron beam welds of an α + β-titanium alloy. J Mater Sci 1996;31:3769–75.
[6] Short AB. Gas tungsten arc welding of α+β titanium alloys: a review. Mater Sci Tech 2009;25:309–24.
[7] Yunlian Q, Ju D, Quan H, Liying Z. Electron beam welding, laser beam welding and gas tungsten arc welding of titanium sheet. Mater Sci Eng A 2000;280:177–81.
[8] Li X, Xie J, Zhou Y. Effects of oxygen contamination in the argon shielding gas in laser welding of commercially pure titanium thin sheet. J Mater Sci 2005;40:3437–43.

[9] Caiazzo F, Curcio F, Daurelio G, Minutolo FMC. Ti6Al4V sheets lap and butt joints carried out by CO2 laser: mechanical and morphological characterization. J Mater Process Tech 2004;149:546–52.
[10] Wang SH, Wei MD, Tsay LW. Tensile properties of LBW welds in Ti–6Al–4V alloy at evaluated temperatures below 450 °C. Mater Lett 2003;57:1815–23.
[11] Du H, Hu L, Liu J, Hu X. A study on the metal flow in full penetration laser beam welding for titanium alloy. Comp Mater Sci 2004;29:419–27.
[12] Li C, Muneharua K, Takao S, Kouji H. Fiber laser-GMA hybrid welding of commercially pure titanium. Mater Des 2009;30: 109–14.
[13] Yu L, Nakata K, Yamamoto N, Liao J. Texture and its effect on mechanical properties in fiber laser weld of a fine-grained Mg alloy. Mater Lett 2009;63:870–2.
[14] Kou S. Welding metallurgy. 2nd ed. New Jersey: John Wiley & Sons Inc.; 2003.
[15] Leary RK, Merson E, Birmingham K, Harvey D, Brydson R. Microstructural and microtextural analysis of InterPulse GTCAW welds in Cp–Ti and Ti–6Al–4V. Mater Sci Eng A 2010;527:7694–705.
[16] Burgers WG. On the process of transition of the cubic-body-centered modification into the hexagonal-close-packed modification of zirconium. Physica 1934;1:561–86.
[17] Gey N, Humbert M. Characterization of the variant selection occurring during the $\alpha \rightarrow \beta \rightarrow \alpha$ phase transformations of a cold rolled titanium sheet. Acta Mater 2002;50:277–87.
[18] Wang SC, Aindow M, Starink MJ. Effect of self-accommodation on α/α boundary populations in pure titanium. Acta Mater 2003;51:2485–503.
[19] Germain L, Gey N, Humbert M. Reliability of reconstructed β-orientation maps in titanium alloys. Ultramicroscopy 2007;107:1129–35.
[20] Gey N, Humbert M. Specific analysis of EBSD data to study the texture inheritance due to the $\beta \rightarrow \alpha$ phase transformation. J Mater Sci 2003;38:1289–94.
[21] Kim SK, Park JK. In-situ measurement of continuous cooling $\beta \rightarrow \alpha$ transformation behavior of CP–Ti. Metall Mater Trans A 2002;33:1051–6.
[22] Oh MS, Lee J-Y, Park JK. Continuous cooling β-to-α transformation behaviors of extra-pure and commercially pure Ti. Metall Mater Trans A 2004;35: 3071–7.
[23] Ahmed T, Rack HJ. Phase transformations during cooling in $\alpha+\beta$ titanium alloys. Mater Sci Eng A 1998;243:206–11.
[24] Plichta MR, Williams JC, Aaronson HI. On the existence of the $\beta \rightarrow \alpha$m transformation in the alloy systems Ti–Ag, Ti–Au, and Ti–Si. Metall Mater Trans A 1977;8:1885–92.
[25] Elmer JW, Wong J, Ressler T. Spatially resolved X-ray diffraction phase mapping and $\alpha \rightarrow \beta \rightarrow \alpha$ transformation kinetics in the heat-affected zone of commercially pure titanium arc welds. Metall Mater Trans A 1998;29:2761–73.
[26] Plichta MR, Aaronson HI, Perepezko JH. The thermodynamics and kinetics of the $\beta \rightarrow \alpha$m transformation in three Ti–X systems. Acta Mater 1978;26:1293–305.
[27] Porter DA, Easterling KE. Phase transformations in metals and alloys. 2nd ed. London: Chapan & Hall; 1992.